$\mathcal{F}$-statistic search for white-dwarf binaries in the first Mock LISA Data Challenge‡

Reinhard Prix and John T Whelan

Max-Planck-Institut für Gravitationsphysik (Albert-Einstein-Institut), D-14476 Potsdam, Germany

Abstract. The $\mathcal{F}$-statistic is an optimal detection statistic for continuous gravitational waves, i.e. long-duration (quasi-)monochromatic signals with slowly-varying intrinsic frequency. This method was originally developed in the context of ground-based detectors, but it is equally applicable to LISA where many signals fall into this class of signals. We report on the application of a LIGO/GEO $\mathcal{F}$-statistic code to LISA data-analysis using the long-wavelength limit (LWL), and we present results of our search for white-dwarf binary signals in the first Mock LISA Data Challenge. Somewhat surprisingly, the LWL is found to be sufficient – even at high frequencies – for *detection* of signals and their accurate localization on the sky and in frequency, while a more accurate modelling of the TDI response only seems necessary to correctly estimate the four amplitude parameters.

E-mail: `reinhard.prix@aei.mpg.de, john.whelan@aei.mpg.de`

1. Introduction

The Mock LISA Data Challenge (MLDC) [1] has the purpose of encouraging the development of LISA data-analysis tools and assessing the technical readiness of the community to perform gravitational-wave (GW) astronomy with LISA. The first round of the MLDC was released in June 2006 [2], the submission deadline was in December 2006 and a report summarizing the submitted results has been published [3]. The challenges consisted of several data-sets containing different types of simulated sources and LISA noise. The three types of sources are white-dwarf binary signals (WD), coalescing supermassive black holes (SMBHs) and extreme mass-ratio inspirals (EMRIs).

The data analysis of LISA poses a few specific difficulties not encountered in ground-based detectors: the signal wavelength is typically not long compared to the arm-length of the detector, so the long-wavelength limit (LWL) does not generally apply. Furthermore, in order to cancel the dominating laser-frequency noise, one has to analyze intricate algebraic combinations of time-delays between spacecraft instead of simple "strain", an approach known as *time-delay interferometry* (TDI). Another difficulty stems from the large number of detectable sources in the LISA bandwidth, which complicates their separate detection and parameter estimation, usually referred to as the "confusion problem".

All of the MLDC signals (WD, SMBH, EMRI) are long-lasting (of the order of a year) and are (quasi-)monochromatic with slowly-varying intrinsic frequency

‡ LIGO-P070029-00-Z

$f(\tau)$; in this sense they belong to the class of *continuous GWs*. In the case of ground-based detectors the typical sources of continuous GWs are spinning neutron stars with non-axisymmetric deformations. One of the standard tools developed for these searches is the $\mathcal{F}$-statistic [4], which is an optimal detection statistic based on matched filtering. We have restricted our searches in the first MLDC to WD-binary signals, which are very similar to GWs from spinning neutron stars, which have very little intrinsic frequency evolution $\dot{f}$ (in fact, here it was $\dot{f} = 0$) and constant orientation and polarization. Contrary to the approach used in [5, 6], we use an $\mathcal{F}$-statistic code developed for the continuous-wave search in LIGO/GEO, with only minimal modifications to adapt it to LISA. In particular, we use the LWL at all frequencies, which turns out to work surprisingly well even at high frequencies where the wavelength is comparable to the LISA arm length.

2. Methods and Pipeline

2.1. Continuous Gravitational Wave Signals

A system with an oscillating mass quadrupole moment emits GWs described, far from the source, by the metric perturbation

$$\overleftrightarrow{h} = A_+ \cos(\phi_0 + \phi)\, \overleftrightarrow{e}_+ + A_\times \sin(\phi_0 + \phi)\, \overleftrightarrow{e}_\times \,, \tag{1}$$

where $\overleftrightarrow{e}_+ = \vec{e}_x \otimes \vec{e}_x - \vec{e}_y \otimes \vec{e}_y$ and $\overleftrightarrow{e}_\times = \vec{e}_x \otimes \vec{e}_y + \vec{e}_y \otimes \vec{e}_x$ are the polarization basis tensors constructed from a right-handed basis $\{\vec{e}_x, \vec{e}_y, \vec{e}_z\}$ with $\vec{e}_z$ pointing in the direction of propagation of the wave, described by the ecliptic longitude λ and latitude β, and $\vec{e}_x$ and $\vec{e}_y$ along the principal polarization axes. In an inertial reference frame, such as the solar-system barycenter (SSB), the phase of this (quasi-)periodic signal can be written as $\phi(\tau) = 2\pi \int_{\tau_{\rm ref}}^{\tau} f(\tau')\, d\tau'$, in terms of the (slowly-varying) intrinsic GW frequency $f(\tau) = f(\tau_{\rm ref}) + \dot{f}(\tau_{\rm ref})\, \Delta\tau + \ldots$. The WD signals in the first MLDC were restricted to have a constant intrinsic frequency, i.e. $f(\tau) = f$. In the case of a binary system for which orbital evolution due to GW emission can be neglected, the principal polarization axes are found by taking the unit vector $\vec{e}_x$ to lie in the orbital plane and $\vec{e}_y$ in the hemisphere containing the orbital angular momentum. The polarization amplitudes are $A_+ = h_0(1 + \cos^2\iota)/2$ and $A_\times = h_0 \cos\iota$, where h_0 is usually referred to as the *amplitude* of the GW, and ι is the inclination angle between the propagation direction $\vec{e}_z$ and the normal to the orbital plane. In order to separate the sky position λ, β from the source polarization, it is useful to consider a polarization basis associated only with the sky position; this is done by defining a right-handed orthonormal basis $\{\vec{e}_\xi, \vec{e}_\eta, \vec{e}_\zeta\}$ with $\vec{e}_\zeta = \vec{e}_z$ as the propagation direction, $\vec{e}_\xi$ lying in the ecliptic plane and $\vec{e}_\eta$ in the northern hemisphere. The alternate polarization basis is then $\overleftrightarrow{\varepsilon}_+ = \vec{e}_\xi \otimes \vec{e}_\xi - \vec{e}_\eta \otimes \vec{e}_\eta$ and $\overleftrightarrow{\varepsilon}_\times = \vec{e}_\xi \otimes \vec{e}_\eta + \vec{e}_\eta \otimes \vec{e}_\xi$, and the principal polarization axes of the GW are determined by the angle ψ from $\vec{e}_\xi$ to $\vec{e}_x$, measured counter-clockwise around $\vec{e}_z = \vec{e}_\zeta$, i.e.

$$\begin{aligned} \overleftrightarrow{e}_+ &= \quad \overleftrightarrow{\varepsilon}_+ \cos 2\psi + \overleftrightarrow{\varepsilon}_\times \sin 2\psi \,, \\ \overleftrightarrow{e}_\times &= -\overleftrightarrow{\varepsilon}_+ \sin 2\psi + \overleftrightarrow{\varepsilon}_\times \cos 2\psi \,. \end{aligned} \tag{2}$$

In terms of this alternative polarization basis, the GW tensor can be written as

$$\overleftrightarrow{h}(\tau) = \sum_{\mu=1}^{4} \mathcal{A}^\mu\, \overleftrightarrow{h}_\mu(\tau) \,, \tag{3}$$

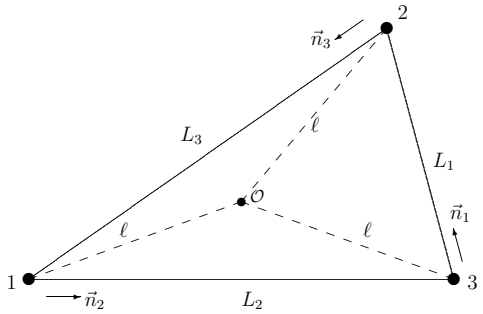

Figure 1. LISA configuration and TDI conventions used.

where the four *amplitude parameters* $\{\mathcal{A}^\mu\}$ are

$$\begin{aligned}
\mathcal{A}^1 &= A_+ \cos\phi_0 \cos 2\psi - A_\times \sin\phi_0 \sin 2\psi \,, \\
\mathcal{A}^2 &= A_+ \cos\phi_0 \sin 2\psi + A_\times \sin\phi_0 \cos 2\psi \,, \\
\mathcal{A}^3 &= -A_+ \sin\phi_0 \cos 2\psi - A_\times \cos\phi_0 \sin 2\psi \,, \\
\mathcal{A}^4 &= -A_+ \sin\phi_0 \sin 2\psi + A_\times \cos\phi_0 \cos 2\psi \,,
\end{aligned} \tag{4}$$

while the tensors $\{\overleftrightarrow{h}_\mu\}$ depend the frequency $f(\tau)$ and the sky position λ, β, namely

$$\begin{aligned}
\overleftrightarrow{h}_1(\tau) &= \overleftrightarrow{\varepsilon}_+ \cos\phi(\tau) \,, \qquad & \overleftrightarrow{h}_2(\tau) &= \overleftrightarrow{\varepsilon}_\times \cos\phi(\tau) \,, \\
\overleftrightarrow{h}_3(\tau) &= \overleftrightarrow{\varepsilon}_+ \sin\phi(\tau) \,, \qquad & \overleftrightarrow{h}_4(\tau) &= \overleftrightarrow{\varepsilon}_\times \sin\phi(\tau) \,.
\end{aligned} \tag{5}$$

2.2. LISA Response in the Long-Wavelength Limit

The LISA design consists of three spacecraft with laser links between each pair, in a geometry illustrated in figure 1. The MLDC data were generated by two different programs: Synthetic LISA [7] simulates a detector output consisting of Doppler shifts of the LISA lasers due to relative motion of the spacecraft, while LISA simulator [8] simulates the phase differences between laser light following different paths between the spacecraft. In both cases the underlying variables are combined with appropriate time shifts to form TDI observables which cancel the (otherwise dominating) laser frequency noise [9, 10, 5]. One choice of such TDI quantities is the set of three observables $\{X, Y, Z\}$, which were used to publish the data of the first MLDC. These observables, which can be thought of as representing the output of three virtual "detectors" I, are related to the gravitational wave $\overleftrightarrow{h}$ through somewhat involved expressions depending on the frequency and propagation direction of the wave. However, in the LWL approximation, in which the wavelength c/f is assumed to be large compared to the distance between the spacecraft, i.e. $f \ll 10\,\mathrm{mHz}$, the responses can be approximated (assuming $L_1 \approx L_2 \approx L_3 \approx L$) as

$$X^{\mathrm{synthLISA}} = -\frac{4L^2}{c^2}\, \overleftrightarrow{d}^X : \dddot{\overleftrightarrow{h}} \,, \qquad X^{\mathrm{LISAsim}} = -\frac{2L}{c}\, \overleftrightarrow{d}^X : \ddot{\overleftrightarrow{h}} \,, \tag{6}$$

where : denotes the contraction of both tensor indices, and $\overleftrightarrow{d}^X \equiv (\vec{n}_2 \otimes \vec{n}_2 - \vec{n}_3 \otimes \vec{n}_3)/2$ is the usual LWL response tensor for a GW interferometer with arms $\vec{n}_2$ and $\vec{n}_3$. The analogous expressions for Y and Z are obtained by cyclic permutations of the indices

$1 \to 2 \to 3 \to 1$. We define an associated scalar "strain" for each of the detectors $I = X, Y, Z$ as

$$h^I(t) \equiv \overleftrightarrow{d}^I(t) : \overleftrightarrow{h}\,(\tau(t)) \,. \tag{7}$$

The timing relation $\tau(t)$ accounts for the Doppler effect caused by the orbital motion of the detector, namely $\tau(t) = t - \vec{r}\cdot\vec{e}_z/c$, where $\vec{r}(t)$ is the position of the detector with respect to the SSB, and $\vec{e}_z$ is the propagation direction of the GW. Note that in the LWL approximation, we can assume that all virtual detectors follow the same trajectory $\vec{r}(t)$ corresponding to the barycenter of the three spacecraft.

The input to our search code consists of Fourier-transformed data stretches of duration T_{SFT}, the so-called SFTs, which is a common data format used within the LIGO Scientific Collaboration for continuous-wave searches (e.g. see [11]). The time baseline T_{SFT} has to be chosen sufficiently short such that the noise-floor can be approximated as stationary and the rotation and acceleration of the detector can be neglected. For LISA we chose $T_{\mathrm{SFT}} = 7\,\mathrm{days}$, while in LIGO/GEO (where the rotation of the Earth dominates the acceleration) this is typically $T_{\mathrm{SFT}} = 30\,\mathrm{min}$. Approximating the detector tensor $\overleftrightarrow{d}^I$ as constant during T_{SFT}, we can Fourier-transform (6) to obtain

$$\widetilde{h}^X(f) = \frac{1}{(4\pi f L/c)^2}\widetilde{X}^{\mathrm{synthLISA}}(f)\,, \quad \widetilde{h}^X(f) = \frac{i}{4\pi f L/c}\widetilde{X}^{\mathrm{LISAsim}}(f)\,. \tag{8}$$

We use $\widetilde{h}^I(f)$ as our SFT input data, and so we can run the same pipeline on LISAsim and synthLISA data, with only a different "calibration" (8) used to generate the SFTs. The noise contributions to X, Y, and Z are correlated, therefore it is often convenient to work with the TDI variables X and $Y - Z$ instead, which are statistically independent. This is a straightforward generalization, using the response tensor $\overleftrightarrow{d}^{Y-Z} = \overleftrightarrow{d}^Y - \overleftrightarrow{d}^Z$.

2.3. The $\mathcal{F}$-Statistic Method

The $\mathcal{F}$-statistic was originally developed in [4] and extended to the multi-detector case in [12]. A generalization to the full TDI framework for LISA was obtained in [5], but here we follow the simpler route of working in the LWL approximation, which allows for a more direct application of existing LIGO/GEO codes to LISA.

Combining the scalar strain (7) with the expression (3) for the GW tensor, we can write the strain signal h^I at detector I as

$$h^I(t) = \sum_{\mu=1}^{4} \mathcal{A}^\mu\, h^I_\mu(t)\,, \tag{9}$$

in terms of the four basis functions

$$\begin{aligned} h^I_1(t) &= a^I(t)\,\cos\phi\,(\tau(t))\,, & h^I_2(t) &= b^I(t)\,\cos\phi\,(\tau(t))\,, \\ h^I_3(t) &= a^I(t)\,\sin\phi\,(\tau(t))\,, & h^I_4(t) &= b^I(t)\,\sin\phi\,(\tau(t))\,, \end{aligned} \tag{10}$$

where we defined the antenna-pattern functions $a^I \equiv \overleftrightarrow{d}^I : \overleftrightarrow{\varepsilon}_+$ and $b^I \equiv \overleftrightarrow{d}^I : \overleftrightarrow{\varepsilon}_\times$. The functions $\{h^I_\mu\}$ depend on the sky-position λ, β and the frequency $f(\tau)$ of the source. We see that the signal parameters separate into two classes: (i) the four *amplitude parameters* $\mathcal{A} \equiv \{\mathcal{A}^\mu\}$, and (ii) the *Doppler parameters* $\theta \equiv \{\lambda, \beta, f, \dot{f}, \ddot{f}, ...\}$. We model the output $x^I(t)$ of detector I as a superposition of stationary Gaussian noise

$n^I(t)$ and a signal $h^I(t;\mathcal{A},\theta)$. Following the notation of [12, 13], we write the different data-streams $x^I(t)$ as a vector $\boldsymbol{x}(t)$, and we define the standard multi-detector scalar product as

$$(\boldsymbol{x}|\boldsymbol{y}) = \sum_{I,J} \int_{-\infty}^{\infty} \widetilde{x}^{I*}(f)\, P^{-1}_{IJ}(f)\, \widetilde{y}^{J}(f)\, df\,, \tag{11}$$

where $\widetilde{x}$ is the Fourier-transform, x^* denotes complex conjugation, and the noise-power matrix $P^{IJ}(f)$ is defined as

$$P^{IJ}(f) \equiv \widetilde{\kappa}^{IJ}(f)\,, \quad \text{with} \quad \kappa^{IJ}(t) \equiv E\left[n^I(t)\, n^J(0)\right]\,, \tag{12}$$

where $E[\,]$ is the expectation value. We search for a signal by seeking the parameters $\{\mathcal{A},\theta\}$ which maximize the log-likelihood ratio

$$L(\boldsymbol{x};\mathcal{A},\theta) = (\boldsymbol{x}|\boldsymbol{h}) - \frac{1}{2}(\boldsymbol{h}|\boldsymbol{h}) = \mathcal{A}^\mu(\boldsymbol{x}|\boldsymbol{h}_\mu) - \frac{1}{2}\mathcal{A}^\mu(\boldsymbol{h}_\mu|\boldsymbol{h}_\nu)\mathcal{A}^\nu\,, \tag{13}$$

where here and in the following we use automatic summation over repeated amplitude indices μ,ν. Defining

$$x_\mu(\theta) \equiv (\boldsymbol{x}|\boldsymbol{h}_\mu)\,, \quad \text{and} \quad \mathcal{M}_{\mu\nu}(\theta) \equiv (\boldsymbol{h}_\mu|\boldsymbol{h}_\nu)\,, \tag{14}$$

we see that L is maximized for given θ by the amplitude parameters $\mathcal{A}^\mu_{\mathrm{MLE}} = \mathcal{M}^{\mu\nu}x_\nu$, where $\mathcal{M}^{\mu\nu}$ is the inverse matrix of $\mathcal{M}_{\mu\nu}$. Thus the detection statistic L, maximized over the amplitude parameters $\mathcal{A}$, is

$$\mathcal{F}(\boldsymbol{x};\theta) \equiv \frac{1}{2}\, x_\mu\, \mathcal{M}^{\mu\nu}\, x_\nu\,, \tag{15}$$

which defines the (multi-detector) $\mathcal{F}$-statistic.

2.4. Analysis Pipeline

Our analysis used standard LAL/LALApps software [14] developed for the search for continuous GWs with ground-based detectors, in particular the code `ComputeFStatistic_v2`, which implements the multi-detector $\mathcal{F}$-statistic (15). Only minor modifications were necessary to adapt this code to the analysis of LISA data using the LWL approximation. All white-dwarf binary signals in the first MLDC had constant intrinsic frequency f, so the set of Doppler parameters consisted of $\theta = \{\lambda,\beta,f\}$. We performed a *hierarchical search* that begins with single-detector searches in each of the TDI variables I, looks for coïncident local maxima of $2\mathcal{F}$, and performs a follow-up multi-detector $\mathcal{F}$-statistic search to establish the parameters of all candidate signals. Our initial analysis submitted as an MLDC entry [3] used the TDI-variables X, Y and Z as three "detectors", assuming for simplicity that their correlation matrix $P^{IJ}(f)$ is diagonal. However, given that the corresponding noises are correlated, we subsequently re-ran the search using the *uncorrelated* TDI variables X and $Y-Z$, which did not result in any significant changes in the results, which are presented here. Whether I ranges through $\{X,Y,Z\}$ or $\{X,\, Y-Z\}$, the structure of the pipeline is the same:

(i) Perform a wide-parameter $\mathcal{F}$-statistic search on each data stream I over a template grid of Doppler parameters $\{\lambda,\beta,f\}$. Keep only candidates which are *local maxima* of $2\mathcal{F}$ above some threshold.

(ii) Keep only *coïncident* candidates with consistent Doppler parameters in all detectors I.

(iii) Perform a more finely-gridded multi-detector search around each candidate to increase the accuracy of the parameter estimation.

(iv) Classify each candidate as *primary* if it has the highest $2\mathcal{F}$ value within $\Delta f = 1.4 \times 10^{-4}\, f$, and as *secondary* otherwise.

The last step arises from the empirical observation that a given signal will have secondary "false" $\mathcal{F}$-statistic maxima at frequencies within roughly $\sim 10^{-4}\, f$ but at different sky positions. Only primary candidates were reported, while the secondary candidates were discarded. This is a limitation of our pipeline: given two signals very close in frequency but at different sky positions, it cannot distinguish the peak at the true sky position of the "fainter" source from a secondary maximum of the "brighter" one. This problem is seen particularly in Challenges 1.1.4 and 1.1.5 with signals clustered very densely in frequency.

3. Results

3.1. Challenge 1.1.1: Isolated Binaries

This challenge consisted of three separate data sets, each containing one WD signal at an unspecified sky position and within a given frequency band: 1.1.1a at $\sim 1\,\mathrm{mHz}$, 1.1.1b at $\sim 3\,\mathrm{mHz}$, and 1.1.1c at $\sim 10\,\mathrm{mHz}$. Note that the LWL is only a good approximation for $f \ll 10\,\mathrm{mHz}$, and we therefore expect it to deteriorate significantly in 1.1.1b and 1.1.1c. Nevertheless, in each of the three cases our pipeline recovered

Table 1. Recovery of Doppler parameters in Challenge 1.1.1: the frequency (error Δf) and sky position (error ϕ_{sky}) are accurately estimated even at the highest frequencies.

Challenge	f	β	λ	Δf	ϕ_{sky}
1.1.1a	1.1 mHz	0.30π	1.62π	1.7 nHz	34.8 mrad
1.1.1b	3.0 mHz	-0.03π	1.47π	0.8 nHz	7.1 mrad
1.1.1c	10.6 mHz	-0.04π	1.48π	0.2 nHz	4.4 mrad

a single primary candidate with an SNR above 10, and the Doppler parameters were determined with very good accuracy, as summarized in table 1. The recovery of the amplitude parameters $\mathcal{A}$ is illustrated in figure 2, comparing the estimated vector $\mathcal{A}_{\mathrm{cand}}$ to the injected parameters $\mathcal{A}_{\mathrm{key}}$. The amplitude four-vectors $\mathcal{A}$ live in a space with constant metric tensor $\mathcal{M}_{\mu\nu}$ given in (14), so the magnitude $|\mathcal{A}|$ is

$$|\mathcal{A}| = \sqrt{\mathcal{A}^\mu\, \mathcal{M}_{\mu\nu}\, \mathcal{A}^\mu} = \sqrt{2\mathcal{F}} \equiv \mathrm{SNR}\,, \tag{16}$$

which defines our signal-to-noise ratio (SNR). The two vectors $\mathcal{A}_{\mathrm{cand}}$ and $\mathcal{A}_{\mathrm{key}}$ define a plane, and so we can plot them in two dimensions, with the horizontal and vertical components

$$\mathcal{A}_\parallel = \frac{\mathcal{A}_{\mathrm{key}} \cdot \mathcal{A}}{|\mathcal{A}_{\mathrm{key}}|}\,, \qquad \mathcal{A}_\perp = \left| \mathcal{A} - \mathcal{A}_\parallel \frac{\mathcal{A}_{\mathrm{key}}}{|\mathcal{A}_{\mathrm{key}}|} \right|\,, \tag{17}$$

where the inner product is calculated using the metric $\mathcal{M}_{\mu\nu}$. These components are shown in figure 2, and we see that the agreement of the amplitude parameters deteriorates substantially for higher frequencies, where the LWL approximation breaks down. The difference between the amplitude vectors, $\Delta\mathcal{A} \equiv \mathcal{A}_{\mathrm{cand}} - \mathcal{A}_{\mathrm{key}}$, has a

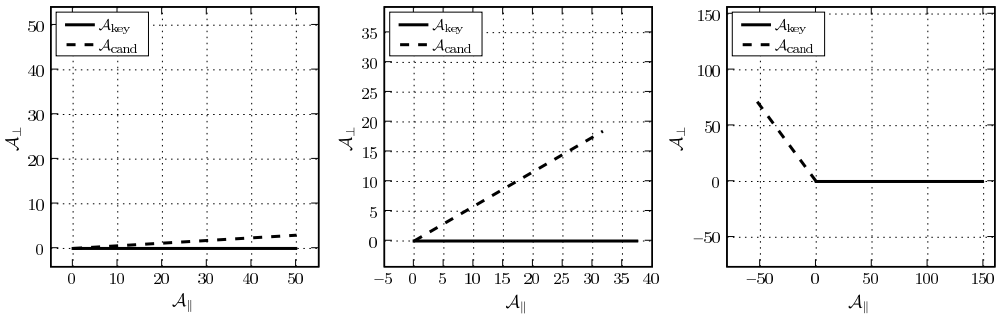

Figure 2. Amplitude parameters for Challenges 1.1.1a (*left*), 1.1.1b (*middle*), and 1.1.1c (*right*). Each plot compares the (4-dimensional) amplitude vectors of the recovered candidate, $\mathcal{A}_{\rm cand}$, to the injected signal, $\mathcal{A}_{\rm key}$, shown in the plane defined by the two vectors. Gaussian fluctuations would lead to a separation of the endpoints of the order $|\Delta\mathcal{A}| \sim 2$. The breakdown of the LWL with increasing frequency leads to larger errors, affecting both the orientation and the length (reflecting the SNR) of the recovered amplitude vector.

covariance matrix $E[\Delta\mathcal{A}^\mu\,\Delta\mathcal{A}^\nu] = \mathcal{M}^{\mu\nu}$, if the deviation is caused by noise *alone*. In this case the magnitude of this difference, i.e. $|\Delta\mathcal{A}| = \sqrt{\Delta\mathcal{A}^\mu\,\mathcal{M}_{\mu\nu}\,\Delta\mathcal{A}^\nu}$, would have variance $E[|\Delta\mathcal{A}|^2] = \mathcal{M}_{\mu\nu}\mathcal{M}^{\mu\nu} = 4$, thus a standard deviation of 2. Table 2

Table 2. Amplitude parameters for Challenge 1.1.1: as seen in figure 2, the angle $\phi_{\mathcal{A}}$ between $\mathcal{A}_{\rm cand}$ and $\mathcal{A}_{\rm key}$ grows with increasing frequency, and there is an increasing deficit in $\mathrm{SNR} = |\mathcal{A}|$. The absolute error from Gaussian noise would be expected to be $|\Delta\mathcal{A}|/2 \sim \mathcal{O}(1)$.

Challenge	f	$\Delta\mathrm{SNR}/\mathrm{SNR}_{\rm key}$	$\phi_{\mathcal{A}}$	$\lvert\Delta\mathcal{A}\rvert/2$
1.1.1a	1.1 mHz	0.005	0.019π	1.5
1.1.1b	3.0 mHz	−0.019	0.168π	9.6
1.1.1c	10.6 mHz	−0.377	0.703π	108.7

summarizes the errors in the amplitude parameters for the three challenge data sets in terms of $|\Delta\mathcal{A}|/2$, the difference in length $\Delta\mathrm{SNR} \equiv \mathrm{SNR}_{\rm cand} - \mathrm{SNR}_{\rm key}$, and the angle $\phi_{\mathcal{A}}$ between the recovered and the injected amplitude vectors, given by

$$\phi_{\mathcal{A}} = \cos^{-1}\left(\frac{\mathcal{A}_{\rm cand}\cdot\mathcal{A}_{\rm key}}{|\mathcal{A}_{\rm cand}|\,|\mathcal{A}_{\rm key}|}\right). \tag{18}$$

We see in table 2 that the amplitude errors are larger than would be expected from noise fluctuations alone, especially at higher frequencies, which is consistent with the breakdown of the LWL.

3.2. Challenge 1.1.2: Verification Binaries

In Challenge 1.1.2, we were provided with the sky positions and frequencies of twenty real and hypothetical "verification binaries" with unspecified amplitude parameters, which were injected into a single data stream. We therefore performed a targeted $\mathcal{F}$-statistic search at each of the specified sets of doppler parameters, and found the maximum-likelihood estimators $\mathcal{A}_{\rm cand}$ for the amplitude parameters. Figure 3

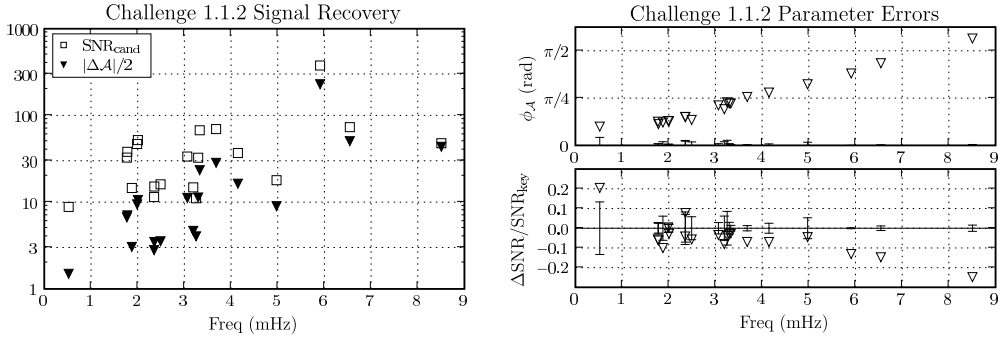

Figure 3. Amplitude parameters for Challenge 1.1.2, where the Doppler parameters were known. *Left:* all 20 signals are recovered with SNR ≥ 8.8, but the errors $|\Delta\mathcal{A}|/2$ are substantially larger than the expected standard deviation of unity for all but the smallest frequencies. *Top right:* the angle $\phi_{\mathcal{A}}$ between the true and recovered amplitude vectors grows with frequency, and is always larger than its expected standard deviation of 1/SNR. *Bottom right:* the length of the recovered amplitude vector is within the expected range for much of the frequency band, but begins to show an SNR deficit above $f > 5\,\mathrm{mHz}$.

illustrates the discrepancies between the recovered amplitude parameters $\mathcal{A}_{\mathrm{cand}}$ and the ones used for the simulation, $\mathcal{A}_{\mathrm{key}}$, in terms of $|\Delta\mathcal{A}|$, $\Delta\mathrm{SNR}/\mathrm{SNR}_{\mathrm{key}}$, and $\phi_{\mathcal{A}}$ used in table 2. Both $\Delta\mathrm{SNR}/\mathrm{SNR}_{\mathrm{key}}$ and $\phi_{\mathcal{A}}$ have expected standard deviations of 1/SNR, and these one-sigma error bars are indicated in the plots on the right. Again we see that our recovered amplitude parameters differ from the injected ones by more than would be expected from Gaussian noise alone, and that the agreement deteriorates at higher frequencies.

3.3. Challenge 1.1.3: Resolvable Binaries

Challenge 1.1.3 was a blind search on data containing 20 white dwarf binary signals across the LISA band. As shown in figure 4, we recovered 17 of the 20 signals with

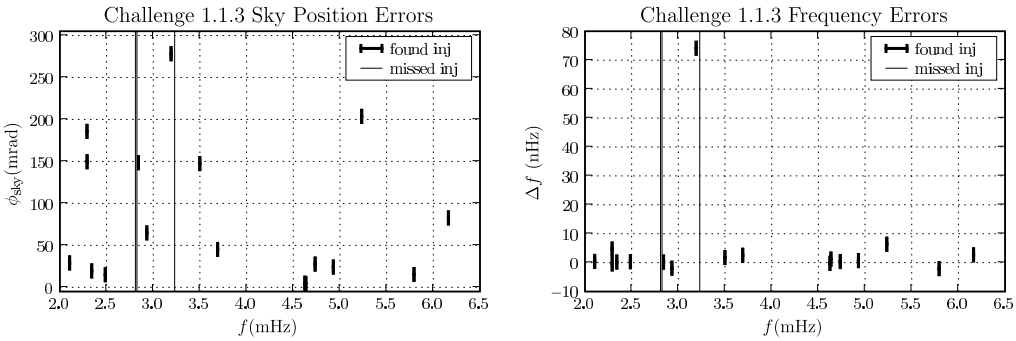

Figure 4. Doppler parameters for Challenge 1.1.3: errors in sky position (*left figure*) and frequency (*right figure*) as functions of frequency. Horizontal errorbars indicate the width of the frequency coïncidence window used, i.e. $1.4 \times 10^{-4} f$, but they are too short to be seen on this scale, making the recovered signals appear as short vertical lines. The three missed signals (long vertical lines) all fall close to recovered signals, but outside of all coïncidence windows.

good frequency and sky accuracy. The three missed signals were at frequencies "close" to recovered sources, but not within the frequency coïncidence window of $1.4 \times 10^{-4} f$, and there is some indication that the Doppler parameters of those sources were slightly compromised.

3.4. Challenge 1.1.4 and 1.1.5: Source Confusion

In Challenges 1.1.4 and 1.1.5, many sources were injected into a small frequency range in order to illustrate the source confusion problem, namely 40–60 signals within [3, 3.015] mHz in Challenge 1.1.4 and 30–50 signals within [2.9985, 3.0015] mHz in Challenge 1.1.5. As shown in Figure 5, our pipeline "found" signals all across the

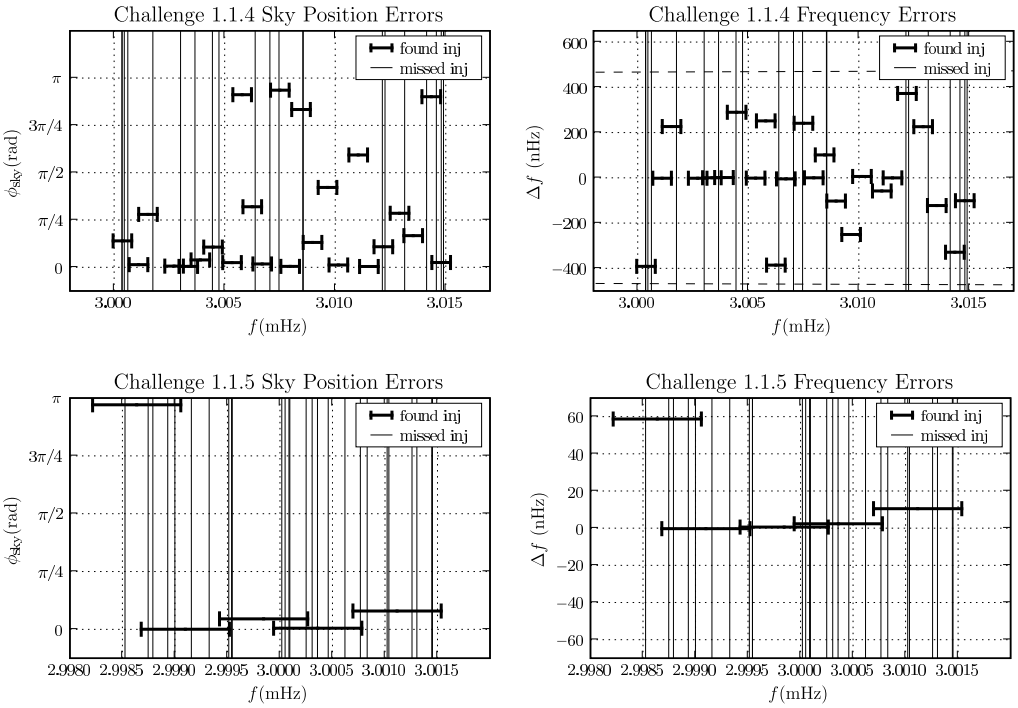

Figure 5. Doppler parameters for Challenges 1.1.4 (*Top row*) and 1.1.5 (*bottom row*): errors in sky position (*left column*) and frequency (*right column*) as functions of frequency. Each of the "missed" injections falls within the coïncidence window of a recovered signal, and would therefore have been rejected as a secondary maximum. The dashed lines in the top-right plot show the maximum possible frequency recovery error, namely the width of the coïncidence window. In both challenges, source confusion causes our pipeline to find a candidate at every possible frequency, including one false alarm at $f = 3.0022$mHz in Challenge 1.1.4.

band, but many of them were far removed in sky position from any true signal. Many additional signals were missed within the frequency coïncidence window, presumably because they were mistaken for secondary maxima of the "found" signals. The results of this challenge illustrate a known limitation of our pipeline: it cannot distinguish multiple signals close together in frequency.

4. Conclusions

Using the $\mathcal{F}$-statistic in the long-wavelength limit approximation, we found that the estimation of the four *amplitude parameters* $\{\mathcal{A}^\mu\}$ deteriorates significantly with increasing frequency, as would be expected from the breakdown of the LWL. However, the *detection* of signals and the estimation of the *Doppler parameters* (frequency and sky-position) does not seem to be affected by the use of the LWL, even at frequencies as high as $f \sim 10\,\mathrm{mHz}$. This somewhat surprising result suggests the following "hierarchical" search strategy: start with a fast $\mathcal{F}$-statistic code using the LWL to detect signals and localize them in Doppler space, then use a more accurate (and computationally expensive) modelling of the TDI responses to estimate the amplitude parameters.

More work is required to deal with "source confusion", i.e. signals that lie within a frequency window $\mathcal{O}(10^{-4}\,f)$. Secondary maxima in parameter space due to a signal cannot easily be distinguished from primary maxima corresponding to other signals within this frequency window. One popular strategy consists of successively "removing" detected signals from the data, which also eliminates its associated secondary maxima, and allows one to re-run the search for the next-loudest candidates. An alternative approach might consist of a classification of candidates into *equivalence classes* consistent with the same signal, either by using the metric or a suitable global correlation criterion analogous to the "circles in the sky" [15] present for short observation times.

Acknowledgments

We thank Stas Babak for a crash course in TDI and Curt Cutler for helpful discussions. This work was supported by the Max-Planck-Society. This paper has been assigned LIGO Document Number LIGO-P070029-00-Z.

References

[1] MLDC homepage. `http://astrogravs.nasa.gov/docs/mldc/`.
[2] K. A. Arnaud et al. 2006. (Preprint `gr-qc/0609105`).
[3] K. A. Arnaud et al. *GWDAW11 Proceedings*, 2007. (Preprint `gr-qc/0701139`).
[4] P. Jaranowski, A. Królak, and B. F. Schutz. *Phys. Rev. D.*, 58:063001, 1998.
[5] A. Królak, M. Tinto, and M. Vallisneri. *Phys. Rev. D.*, 70:022003, 2004.
[6] A. Królak. *Proceedings of GWDAW11*, 2007.
[7] M. Vallisneri. Synthetic LISA Software. `http://www.vallis.org/syntheticlisa/`.
[8] N. J. Cornish and L. Rubbo. The LISA Simulator. `http://www.physics.montana.edu/lisa/`.
[9] J. W. Armstrong, F. B. Estabrook, and M. Tinto. *ApJ*, 527:814–826, 1999.
[10] M. Tinto, F. B. Estabrook, and J. W. Armstrong. *Phys. Rev. D.*, 69:082001–+, 2004.
[11] LIGO Scientific Collaboration. 2006. (Preprint `gr-qc/0605028`).
[12] C. Cutler and B. F. Schutz. *Phys. Rev. D.*, 72:063006, 2005.
[13] R. Prix. *Phys. Rev. D.*, 75:023004, 2007.
[14] LIGO Scientific Collaboration. LAL/LALApps: FreeSoftware (GPL) tools for data-analysis. `http://www.lsc-group.phys.uwm.edu/daswg/`.
[15] R. Prix and Y. Itoh. *Class. Quant. Grav.*, 22:S1003–S1012, 2005.